Supporting Information

In-situ restructuring of Ni-based metal organic frameworks for photocatalytic CO_2 hydrogenation

Abdelaziz Gouda[1,2,3†*], Karen Hannouche[4†], Abhinav Mohan[2,3], Chengliang Mao[1], Ehsan Nikbin[5], Alexandre Carrière [6], Jessica Ye[1], Jane Y. Howe[2,5], Mohini Sain[2,3*], Mohamad Hmadeh[1,4*] and Geoffrey A. Ozin[1,2*]

[1]Department of Chemistry, University of Toronto, 80 St George St, Toronto, ON M5S 3H6, Canada
[2]Department of Chemical Engineering and Applied Chemistry, University of Toronto, 200 College St., Toronto, ON M5S 3E5, Canada
[3]Department of Mechanical and Industrial Engineering, University of Toronto, 5 King's College Rd, Toronto, ON, M5S 3G8, Canada
[4]Department of Chemistry, Faculty of Arts and Sciences, American University of Beirut, P.O. Box 11-0236, Beirut 1107 2020, Lebanon.
[5]Department of Materials Science & Engineering, University of Toronto, 184 College St., M5S 3E4, Toronto, Canada
[6]Department of Engineering Physics, Polytechnique Montreal, Montreal, QC, H3T 1J4 Canada

[†]Authors contributed equally to this work

Corresponding Authors:

Abdelaziz Gouda: abdelaziz.gouda@utoronto.ca

Mohini Sain: m.sain@utoronto.ca

Mohamad Hmadeh: mh210@aub.edu.lb

Geoffrey A. Ozin: g.ozin@utoronto.ca

Table of Contents

1. Characterization of the synthesized MOFs 3

1.1. Structural Analysis 3

1.2. Spectral Analysis and Electronic Structure Elucidation 5

2. LED light source characterization 7

3. Elucidation of the reaction's pathways 8

4. Control experiments for the Ni-Nb catalyzed photocatalytic reaction 12

5. Investigation of the in-situ restructuring process 14

5.1. TEM imaging 14

5.2. Atomic Force Microscopy 15

5.3. Elemental analysis 16

5.4. EDS mapping 18

5.5. Diffuse reflectance spectroscopy (DRS) and Tauc plots analysis 20

5.6. TGA-FTIR 22

5.7. X-Ray photoelectron spectroscopy (XPS) analysis 23

1. Characterization of the synthesized MOFs

1.1. Structural Analysis

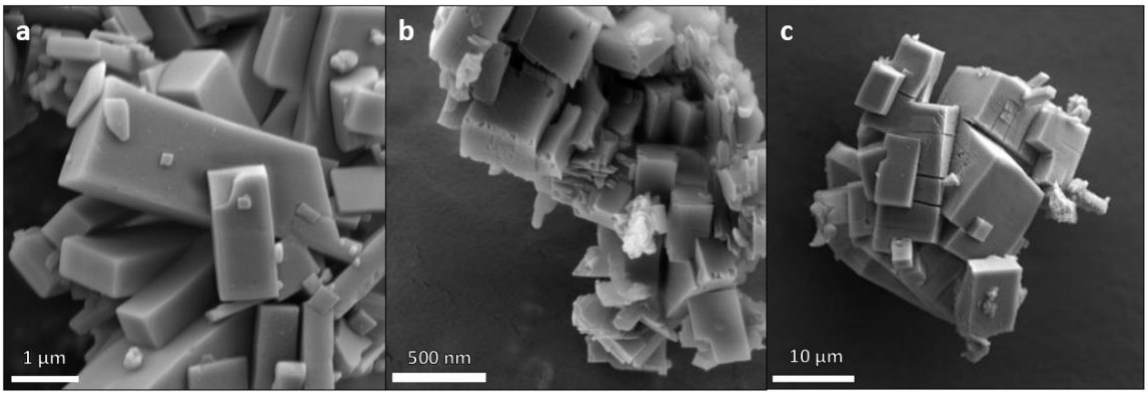

Supplementary Fig. 1. Scanning electron microscopy images of the as synthesized catalysts. SEM images of **a** Ni-Nb MOF, **b** Ni-Al-MOF and **c** Ni-Fe-MOF.

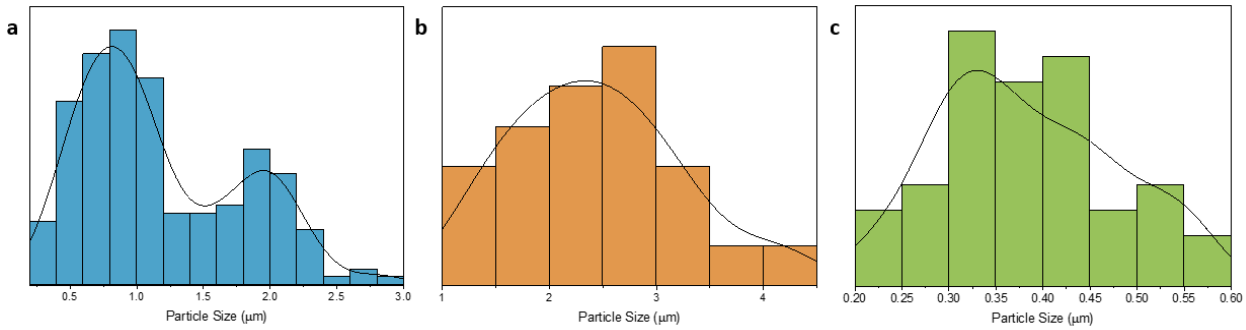

Supplementary Fig. 2. **MOFs particle size distribution**. **a** Ni-Nb-MOF particle size distribution (blue bars), **b** Ni-Al-MOF particle size distribution (orange bars) and **c** Ni-Fe-MOF particle size distribution (green bars) measured from TEM images of the as-synthesized MOFs.

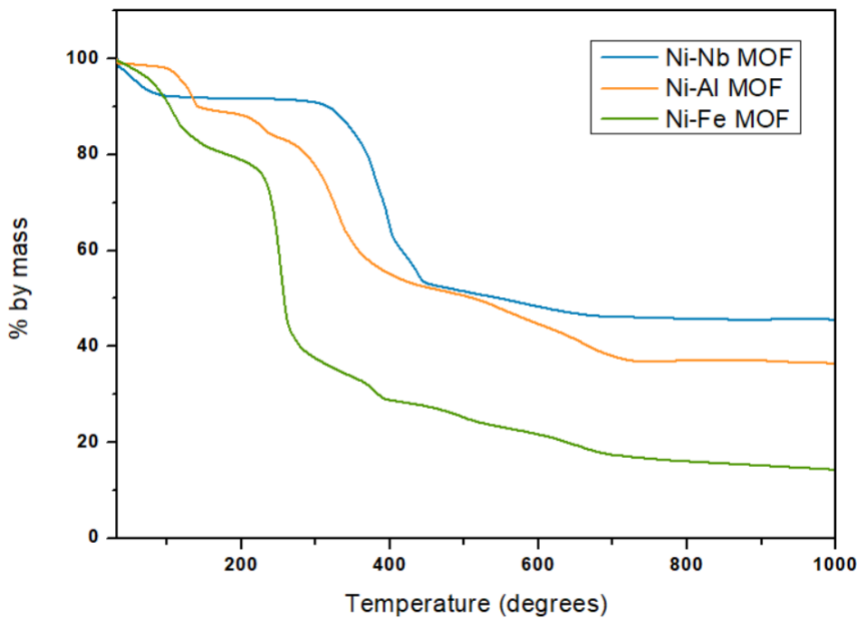

Supplementary Fig. 3. Thermogravimetric analysis. TGA curves of Ni-Nb-MOF (blue line), Ni-Al-MOF (orange line) and Ni-Fe-MOF (green line) performed under N_2 atmosphere at a rate of 10ºC/min.

1.2. Spectral Analysis and Electronic Structure Elucidation

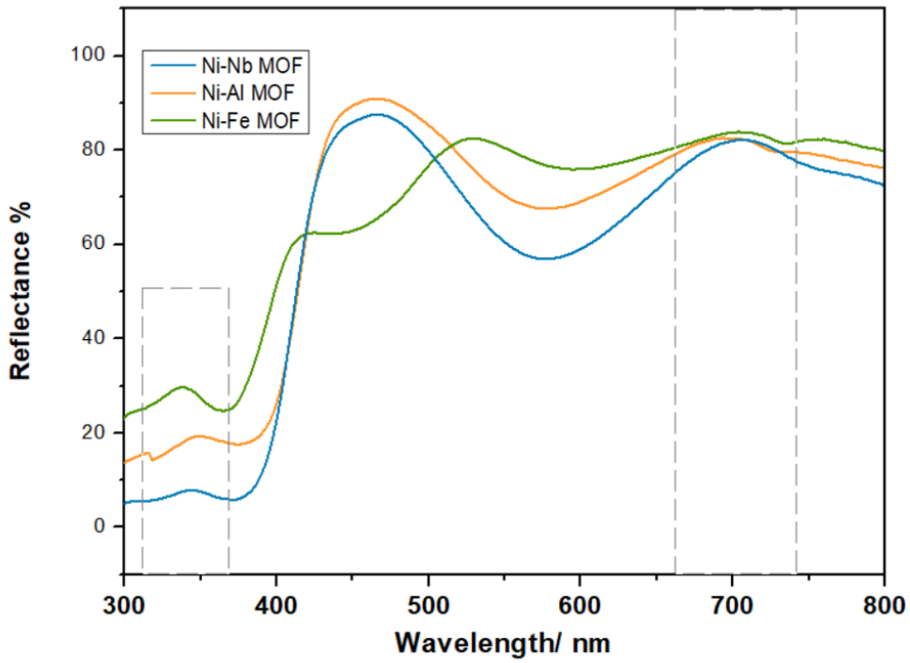

Supplementary Fig. 4. Optical properties of the as-synthesized catalysts. UV-Vis DRS spectra of the as-synthesized Ni-Nb-MOF (blue line), Ni-Al-MOF (orange line) and Ni-Fe-MOF (green line).

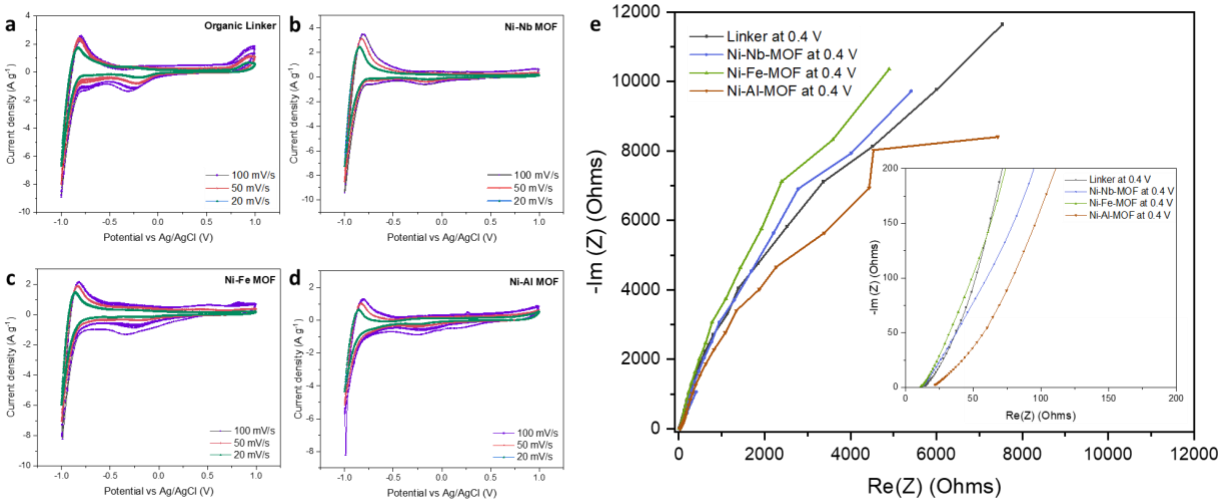

Supplementary Fig. 5. Charge transfer properties of the as-synthesized MOFs. Cyclic voltammograms of **a** pyrazine linker, **b** Ni-Nb MOF, **c** Ni-Fe MOF and **d** Ni-Al MOF measured at 100 mV/s (purple lines), 50 mV/s (pink lines) and 20 mV/s (green lines). **e** Electrochemical impedance spectra of the three studied MOFs (Ni-Nb-MOF in blue, Ni-Al-MOF in orange and Ni-Fe-MOF in green) and their pyrazine linker (black line) in the frequency range 10^5-10^1 Hz. Inset: Zoomed Nyquist plot.

2. LED light source characterization

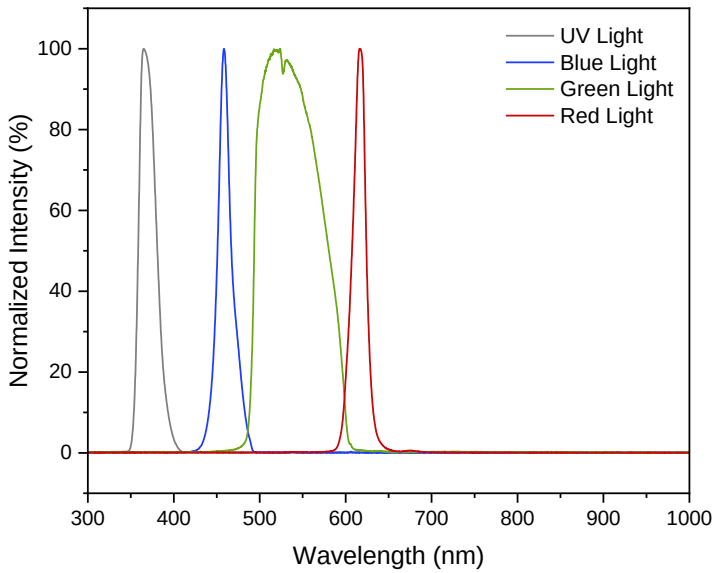

Supplementary Fig. 6. LED source characterization. Emission spectra of the components of LED ligh (UV, blue, green and red light) used in the photocatalytic experiments.

Supplementary Table 1. LED light source irradiance corresponding to different light compositions. (spot area = 1.1 cm^2)

LED light composition				Power (W)	Irradiance (W/cm^2)
UV (%)	Blue (%)	Green (%)	Red (%)		
0	0	0	0	0	0.0
25	25	25	25	1.59	1.4
50	50	50	50	2.89	2.6
75	75	75	75	4.05	3.7
100	100	100	100	5.05	4.6
0	100	100	100	3.45	3.1
25	100	100	100	3.87	3.5
50	100	100	100	4.29	3.9
75	100	100	100	4.68	4.3
100	100	100	100	5.05	4.6
100	0	100	100	2.76	2.5
100	25	100	100	3.52	3.2
100	50	100	100	4.11	3.7

100	75	100	100	4.62	4.2
100	100	100	100	5.05	4.6
100	100	0	100	4.27	3.9
100	100	25	100	4.53	4.1
100	100	50	100	4.72	4.3
100	100	75	100	4.89	4.4
100	100	100	100	5.05	4.6
100	100	100	0	4.62	4.2
100	100	100	25	4.75	4.3
100	100	100	50	4.86	4.4
100	100	100	75	4.95	4.5
100	100	100	100	5.05	4.6

3. Elucidation of the reaction's pathways

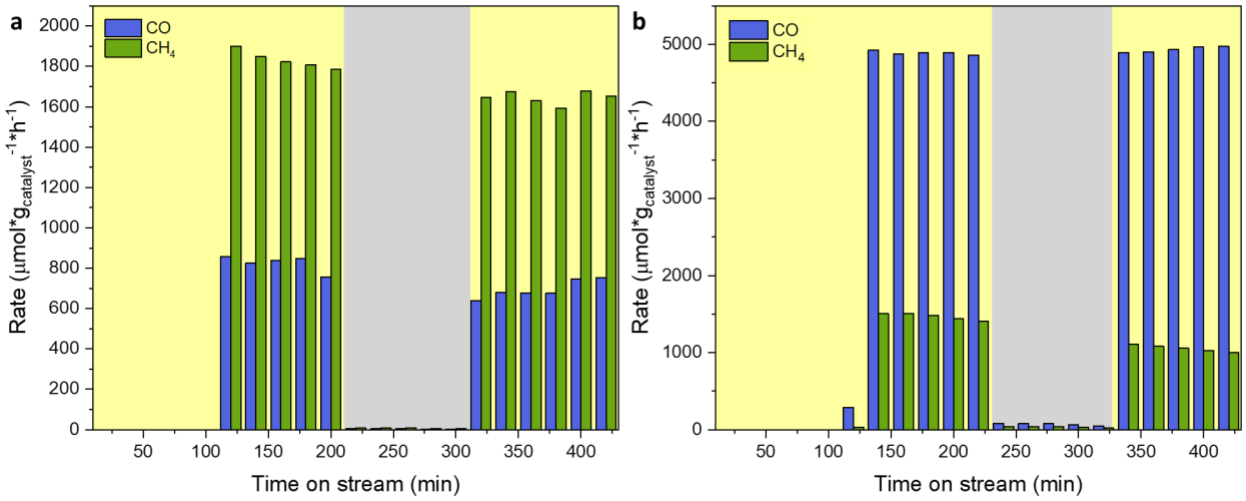

Supplementary Fig. 7. Role of light irradiation in the catalytic reaction. **a** CO (blue bars) and CH_4 (green bars) production rates using Ni-Nb-MOF as a catalyst. **b** CO (blue bars) and CH_4 (green bars) production rates using Ni-Fe-MOF as a catalyst. *Reaction conditions:* 180ºC, (1:1) (CO_2:H_2), yellow-shaded areas under 4.6 W/cm^2 LED light intensity and grey-shaded areas under dark conditions.

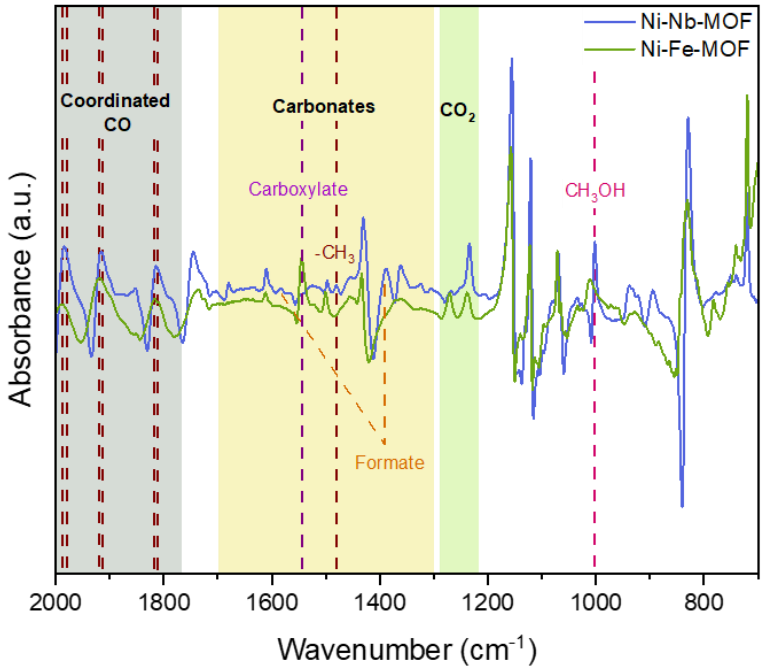

Supplementary Fig. 8. Comparison between in-situ DRIFTS of Ni-Nb and Ni-Fe catalysts. In-situ DRIFTS spectra of Ni-Nb-MOF (blue line) and Ni-Fe-MOF (green line) at 180°C, (1:4) and (1:1) (CO_2 : H_2) respectively, and 4.6 W/cm^2 LED light intensity. Intermediates are identified by dashed lines.

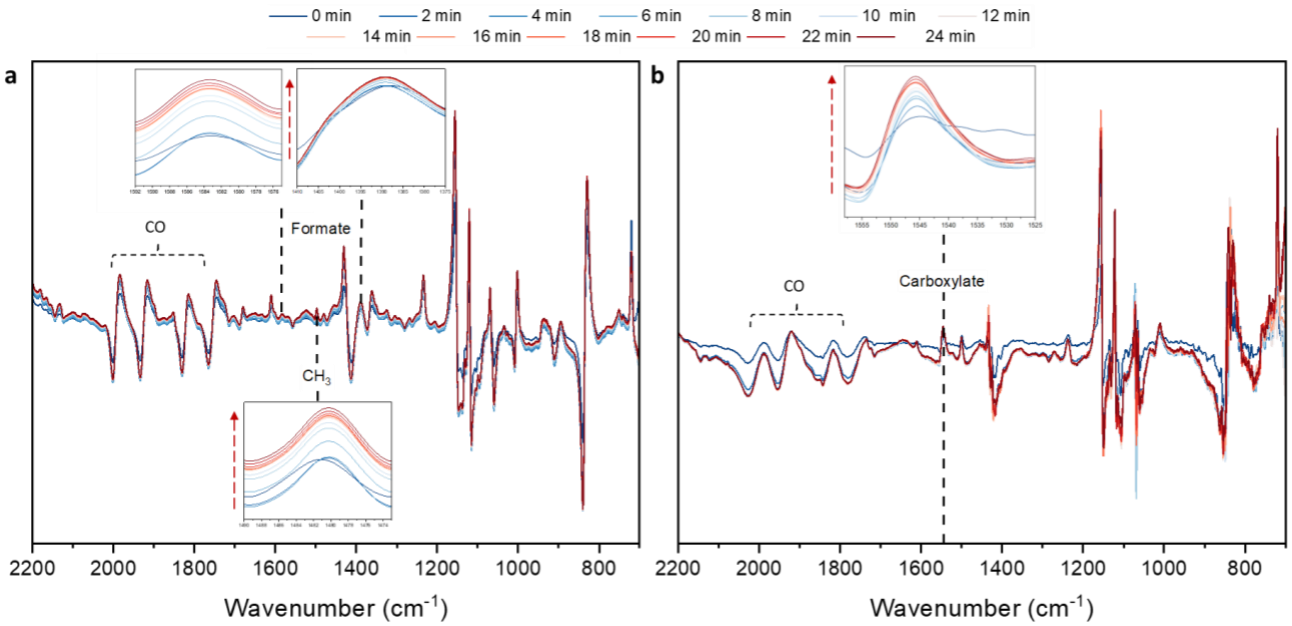

Supplementary Fig. 9. In-situ time-dependent DRIFTS measurements for the identification of intermediates. In-situ DRIFTS spectra of **a** Ni-Nb-MOF and **b** Ni-Fe-MOF, under a flow of (1:4) and (1:1) (CO_2 : H_2) respectively, 180ºC and 4.6 W/cm^2 LED light intensity, recorded every 2 mins for 24 mins after restructuring (blue to red-shaded lines).

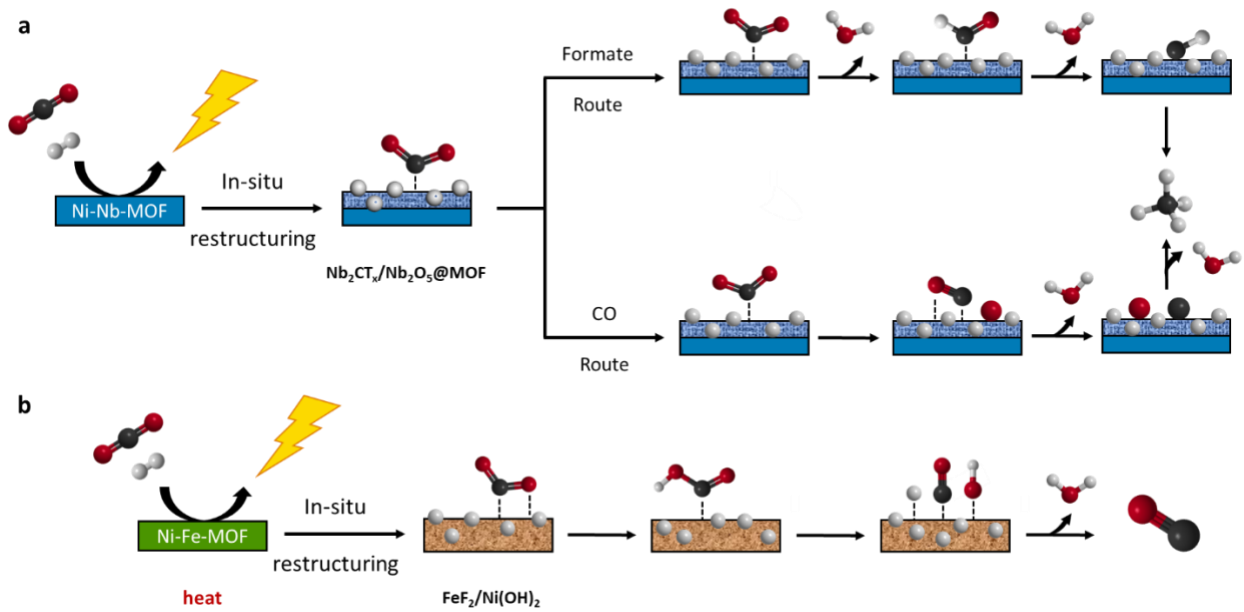

Supplementary Fig. 10. Possible reaction routes. **a** Suggested CH_4 formation pathways on the surface of Ni-Nb-MOF. **b** Suggested CO formation route using Ni-Fe-MOF as a catalyst. *Evidence for the formation of Nb_2CT_x/Nb_2O_5 and $FeF_2/Ni(OH)_2$ will be given in subsequent sections.*

4. Control experiments for the Ni-Nb catalyzed photocatalytic reaction

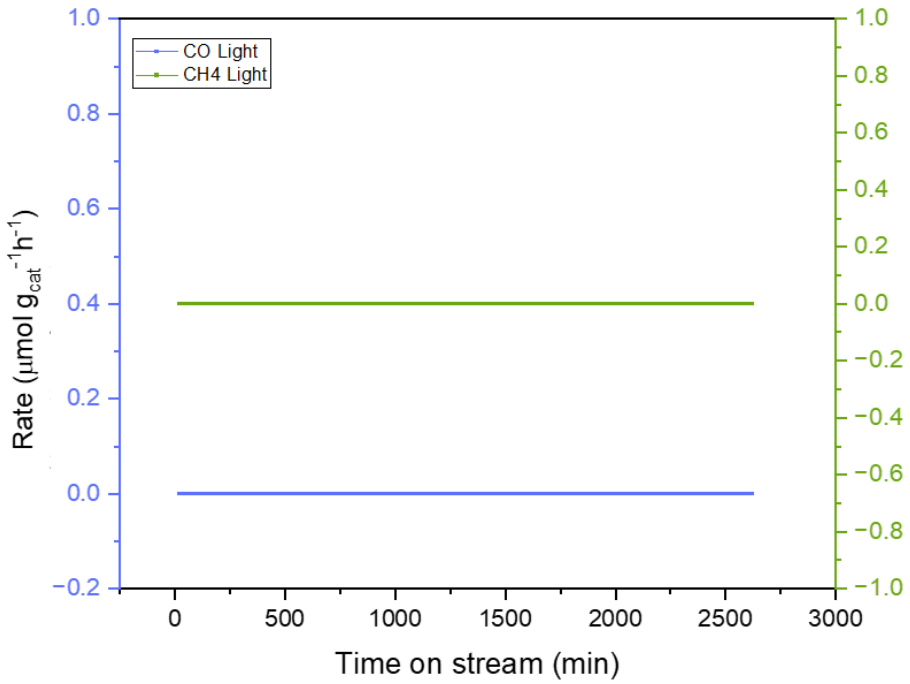

Supplementary Fig. 11. Control experiment. CH_4 (green line) and CO (blue line) formation rates using Ni-Nb-MOF as a catalyst at 180ºC, 4.6 W/cm^2 LED irradiation and in the absence of CO_2.

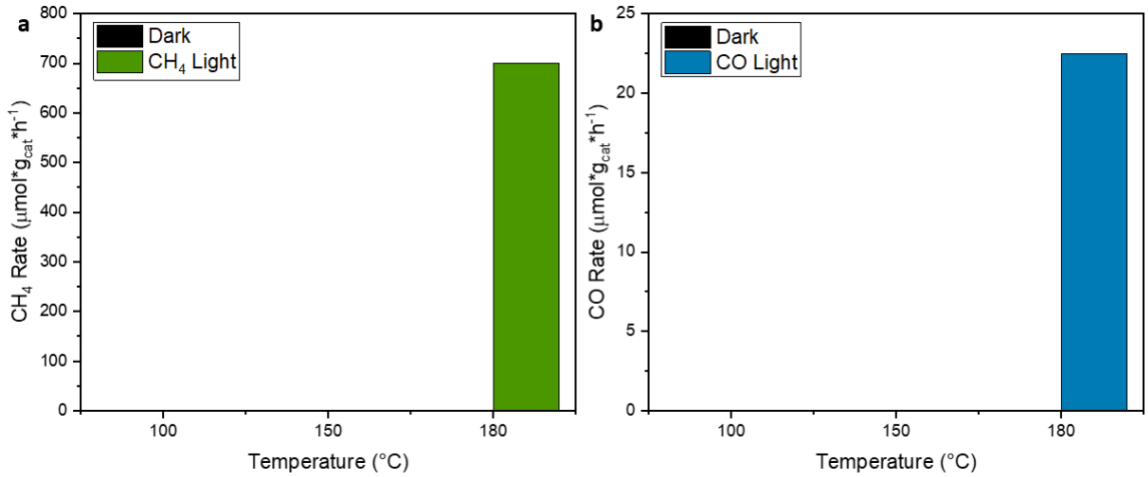

Supplementary Fig. 12. Control experiments a CH_4 production rates (green bars) and **b** CO production rates (blue bars) in the presence and absence of light respectively, both using Ni-Nb-MOF as a catalyst and (1:4) (CO_2:H_2) flow at 180°C..

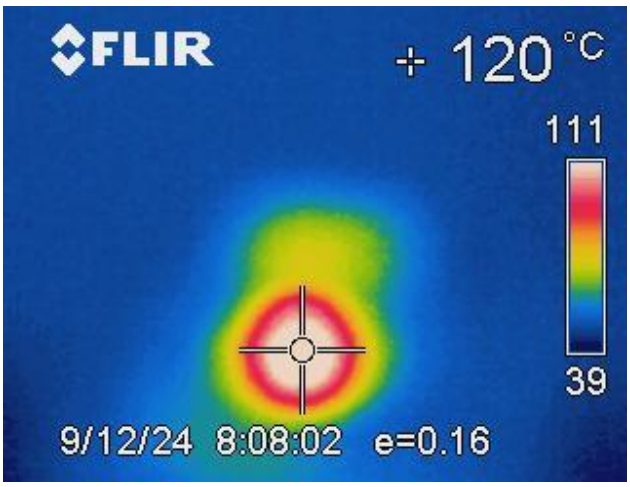

Supplementary Fig. 13. Surface temperature determination. Forward-looking infrared camera image of Ni-Nb-MOF surface without heating, under 4.6 W/cm^2 light irradiation and a flow of (1:4) (CO_2:H_2).

5. Investigation of the in-situ restructuring process

5.1. TEM imaging

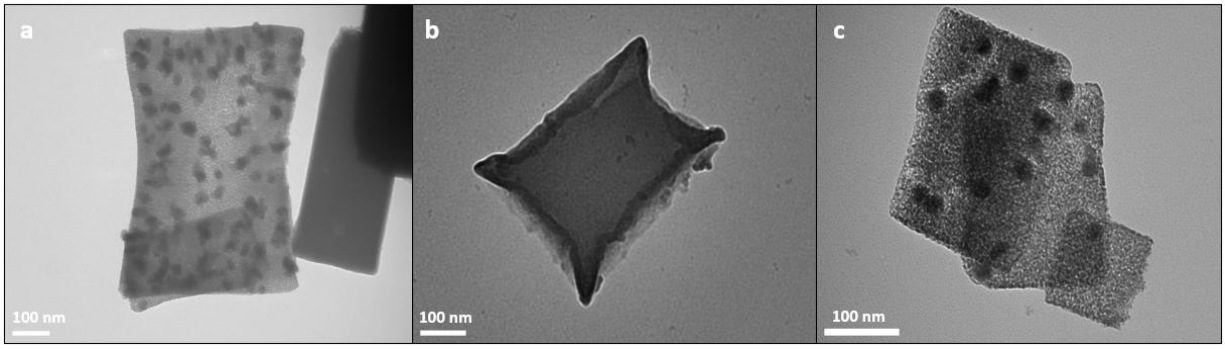

Supplementary Fig. 14. Transmission electron microscopy imaging post-catalysis. TEM images of **a** spent Ni-Nb-MOF, **b** spent Ni-Al-MOF and **c** spent Ni-Fe-MOF.

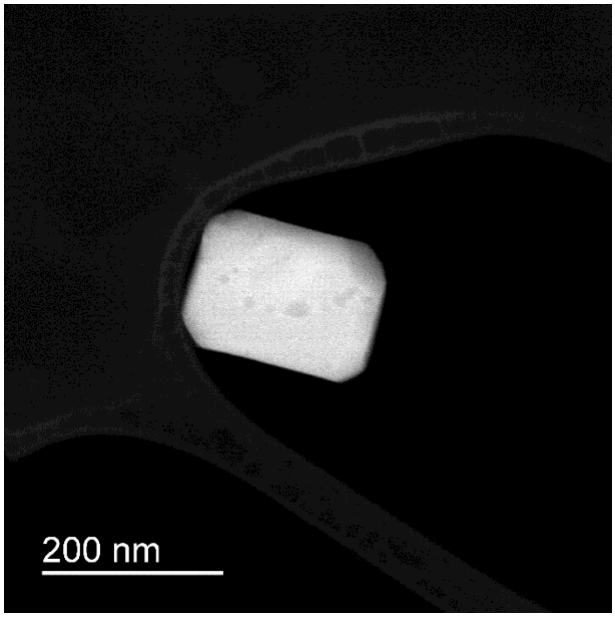

Supplementary Fig. 15. Annular dark field-scanning transmission electron microscopy imaging of Ni-Nb catalyst under thermal conditions. ADF-STEM image of Ni-Nb-MOF after thermal methanation at 300°C.

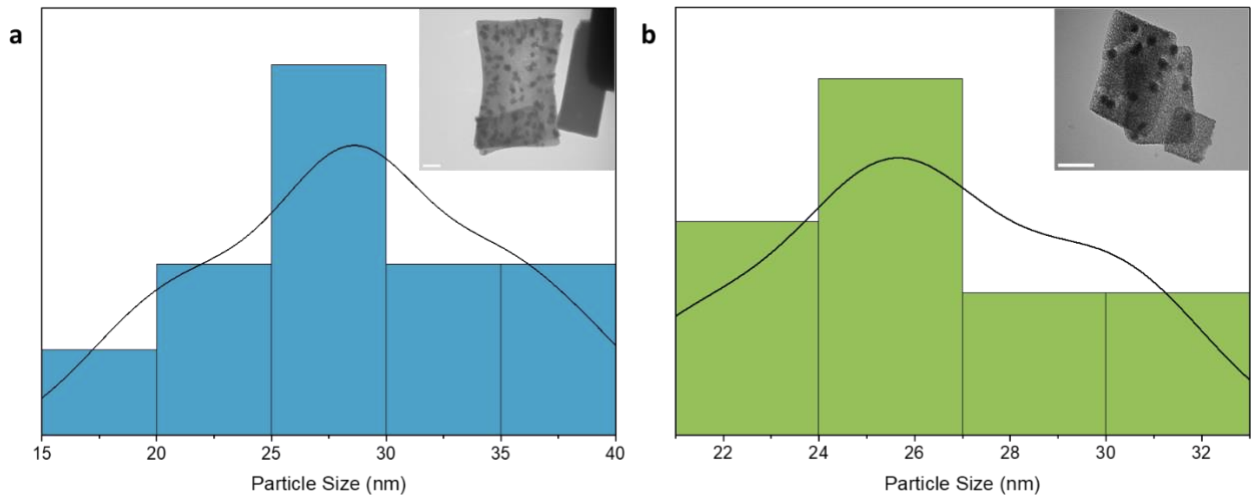

Supplementary Fig.16. Particle size distribution of surface particles. **a** Particle size distribution of the particles formed on the surface of Ni-Nb catalyst throughout the catalytic reaction, represented by blue bars. **b** Particle size distribution of the particles formed on the surface of Ni-Fe catalyst throughout the catalytic reaction, represented by green bars. (Scale bar = 100 nm).

5.2. Atomic Force Microscopy

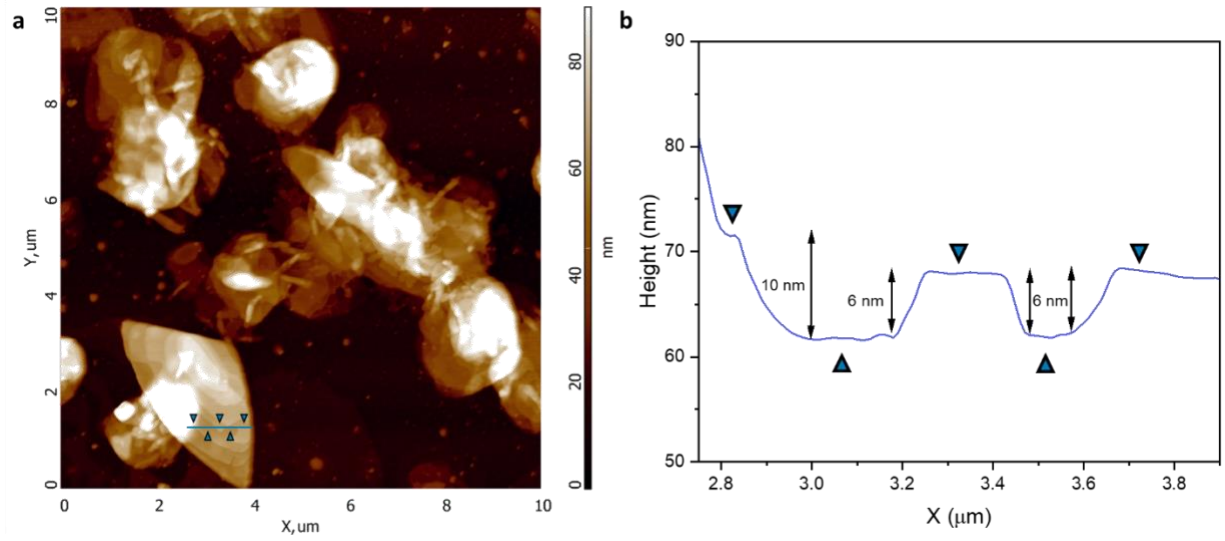

Supplementary Fig. 17. AFM imaging and surface thickness determination. **a** AFM image of Ni-Nb-MOF after catalysis. **b** Height profile of the line highlighted in blue.

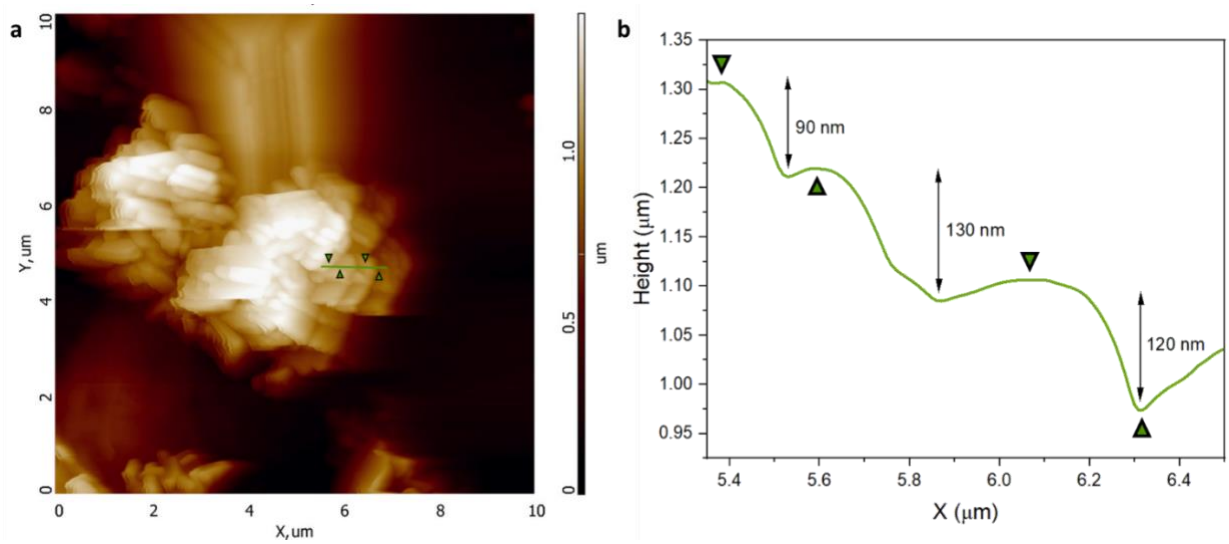

Supplementary Fig. 18. AFM imaging and surface thickness determination. a AFM image of Ni-Fe catalyst after reaction. **b** Height profile of the line highlighted in green.

5.3. Elemental analysis

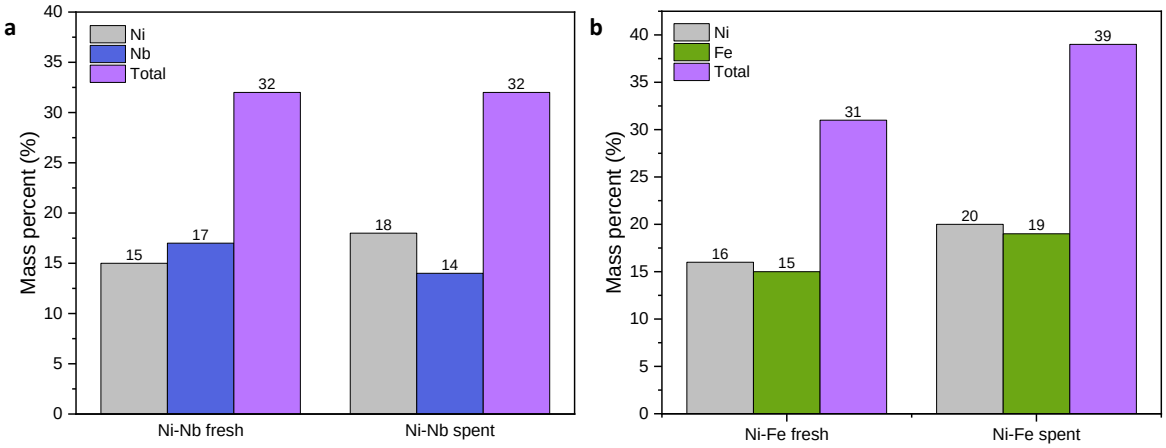

Supplementary Fig. 19. Catalysts' metal composition before and after catalysis. a Ni (grey), Nb (blue) and total (purple) metal composition in Ni-Nb-MOF before and after catalysis. **b** Ni, Fe and total metal composition in Ni-Fe-MOF before and after catalysis.

Supplementary Table 2. Relative metal composition from ICP-OES. Relative metal percentages in Ni-Nb and Ni-Fe catalysts before and after reaction as calculated from ICP-OES.

From ICP					
	Fresh Ni-Nb-MOF	Spent Ni-Nb-MOF		Fresh Ni-Fe-MOF	Spent Ni-Fe-MOF
Ni %	47	56	Ni %	52	51
Nb %	53	44	Fe %	48	49

Supplementary Table 3. Relative metal composition from SEM-EDX. Relative metal percentages in Ni-Nb and Ni-Fe catalysts before and after reaction as calculated from three SEM-EDX measurements for each material.

From EDX					
	Fresh Ni-Nb-MOF	Spent Ni-Nb-MOF		Fresh Ni-Fe-MOF	Spent Ni-Fe-MOF
Ni %	35	41	Ni %	53	52
Nb %	65	59	Fe %	47	48

5.4. EDS mapping

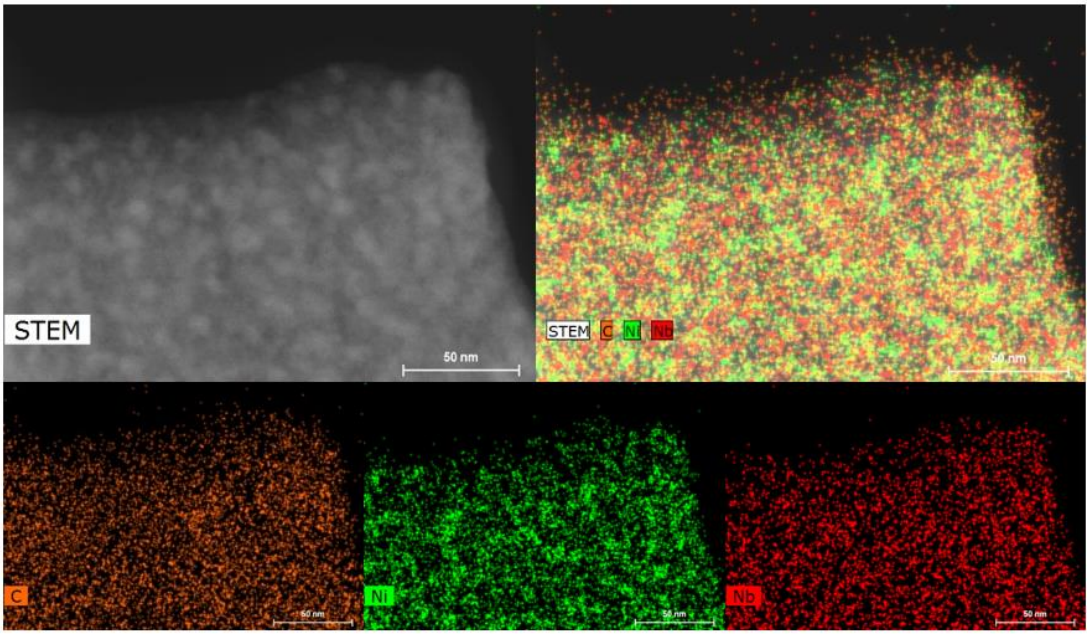

Supplementary Fig. 20. Elemental composition of Ni-Nb-MOF post catalysis. EDS maps showing the distribution of C (orange), Ni (green) and Nb (red) on the surface of Ni-Nb-MOF after reaction.

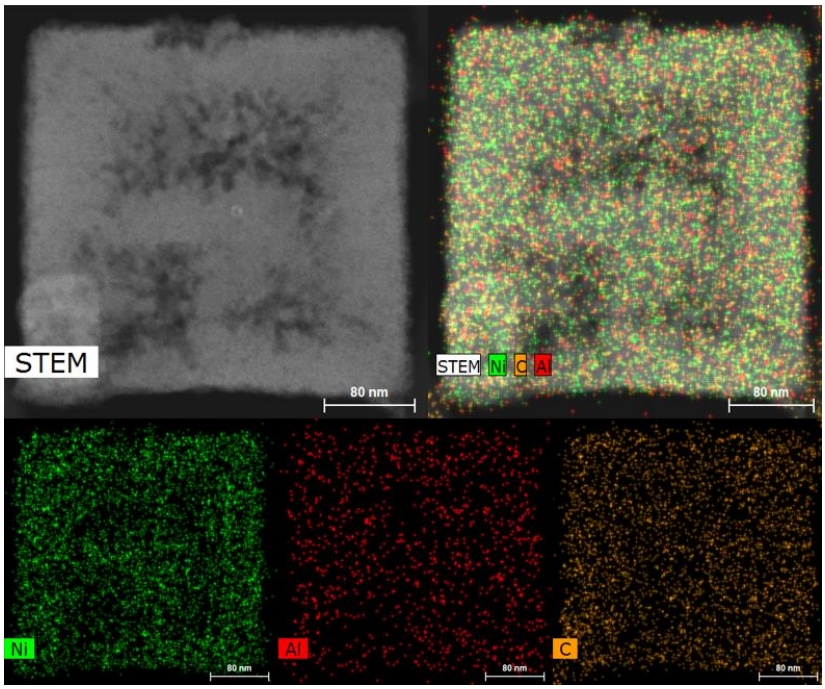

Supplementary Fig. 21. Elemental composition of Ni-Al-MOF post catalysis. EDS maps showing the distribution of Ni (green), Al (red) and C (orange) on the surface of Ni-Al-MOF after reaction.

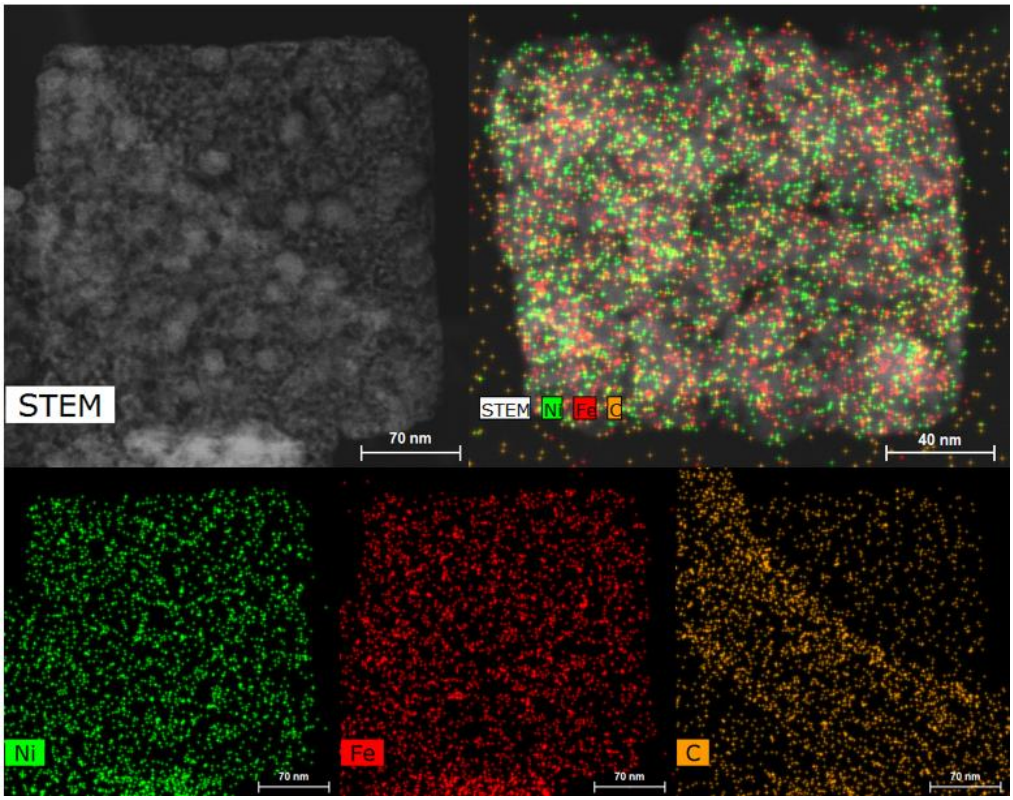

Supplementary Fig. 22. Elemental composition of Ni-Fe-MOF post catalysis. EDS maps showing the distribution of Ni (green), Fe (red) and C (orange) on the surface of Ni-Fe-MOF after reaction.

5.5. Diffuse reflectance spectroscopy (DRS) and Tauc plots analysis

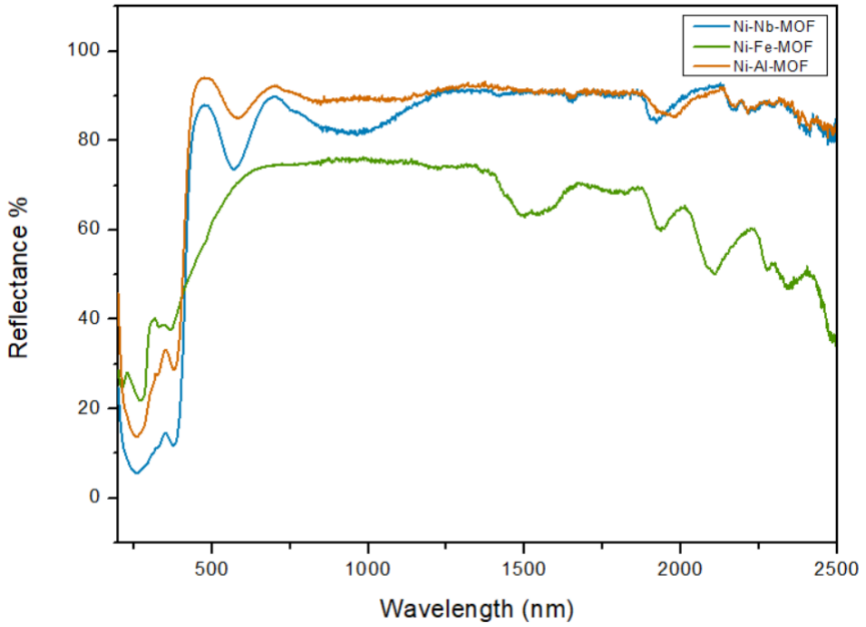

Supplementary Fig. 23. Optical properties of the three MOFs after catalysis. UV-Vis DRS spectra of Ni-Nb-MOF (blue line), Ni-Al-MOF (orange line) and Ni-Fe-MOF (green line) after reaction.

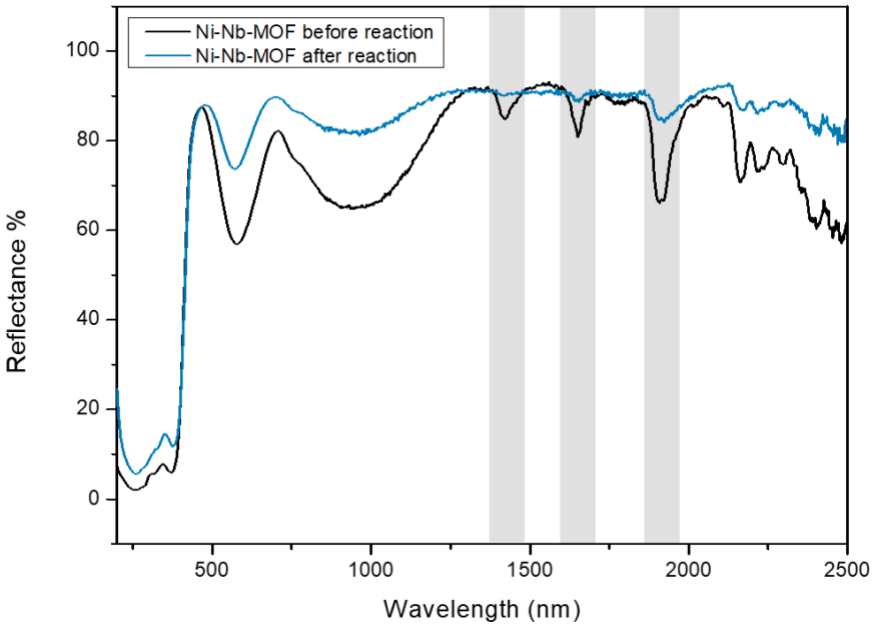

Supplementary Fig. 24. DRS spectra of fresh and spent Ni-Nb-MOF. Comparison between the DRS spectra of Ni-Nb-MOF before (black line) and after (blue line) reaction. Peaks that disappear throughout the reaction are shaded in grey.

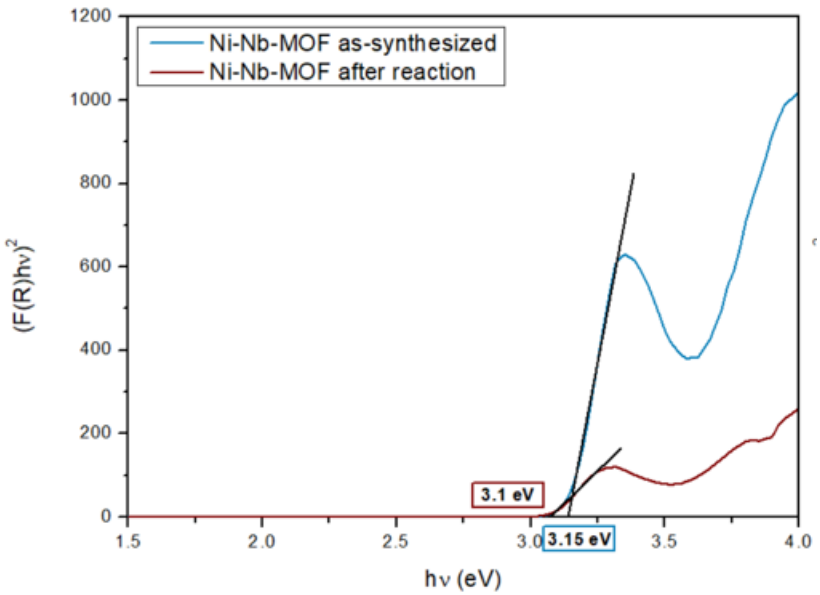

Supplementary Fig. 25. Band gap determination. Optical band gap estimation from tauc plots of Ni-Nb-MOF before (blue line) and after (red line) catalysis.

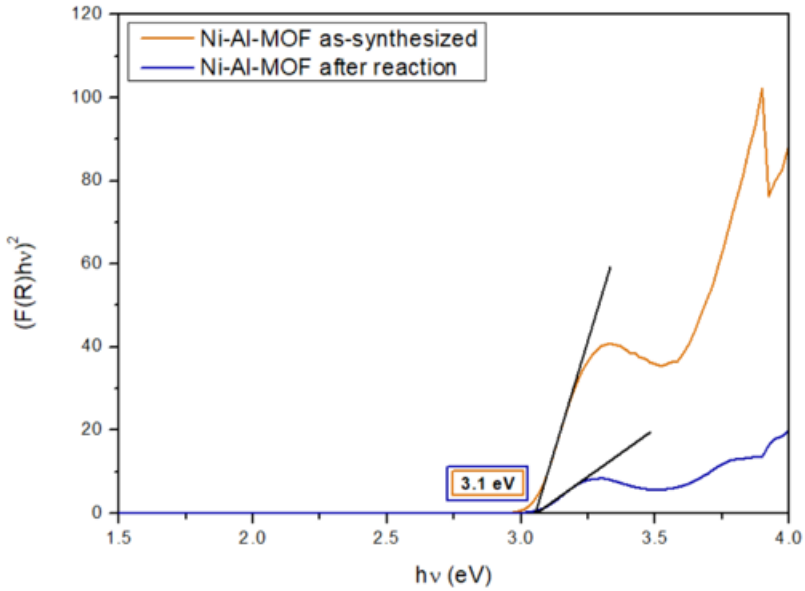

Supplementary Fig. 26. Band gap determination. Optical band gap estimation from tauc plots of Ni-Al-MOF before (orange line) and after (navy line) catalysis.

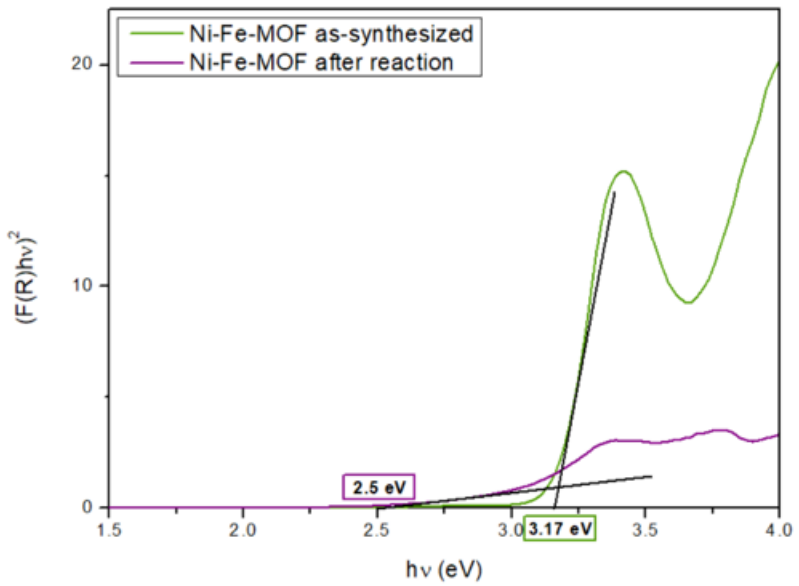

Supplementary Fig. 27. Band gap determination. Optical band gap estimation from tauc plots of Ni-Fe-MOF before (green line) and after (purple line) catalysis.

5.6. TGA-FTIR

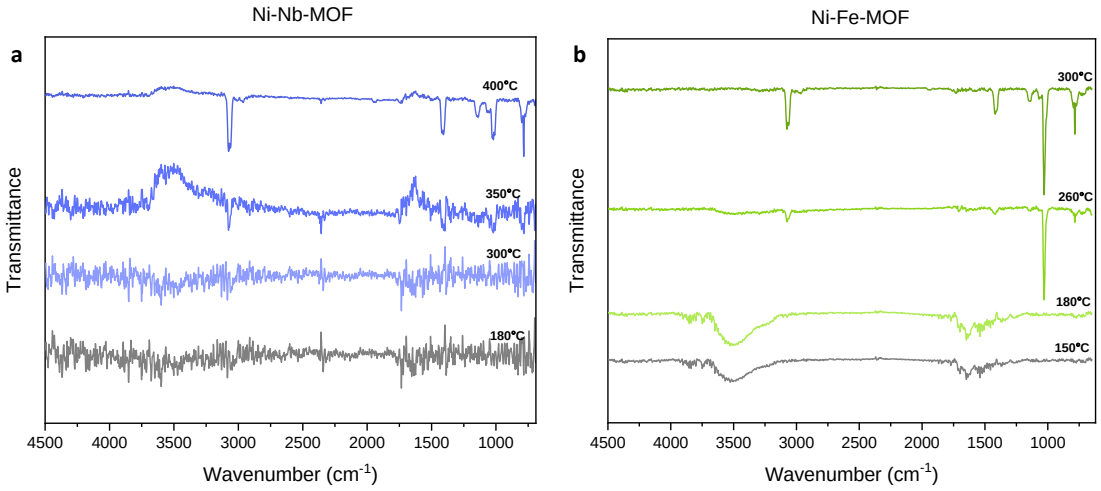

Supplementary Fig. 28. FTIR-coupled TGA. a FTIR spectra of released species upon heating Ni-Nb-MOF at selected temperatures under inert conditions. **b** FTIR spectra of released species upon heating Ni-Fe-MOF at selected temperatures under inert conditions.

5.7. X-Ray photoelectron spectroscopy (XPS) analysis

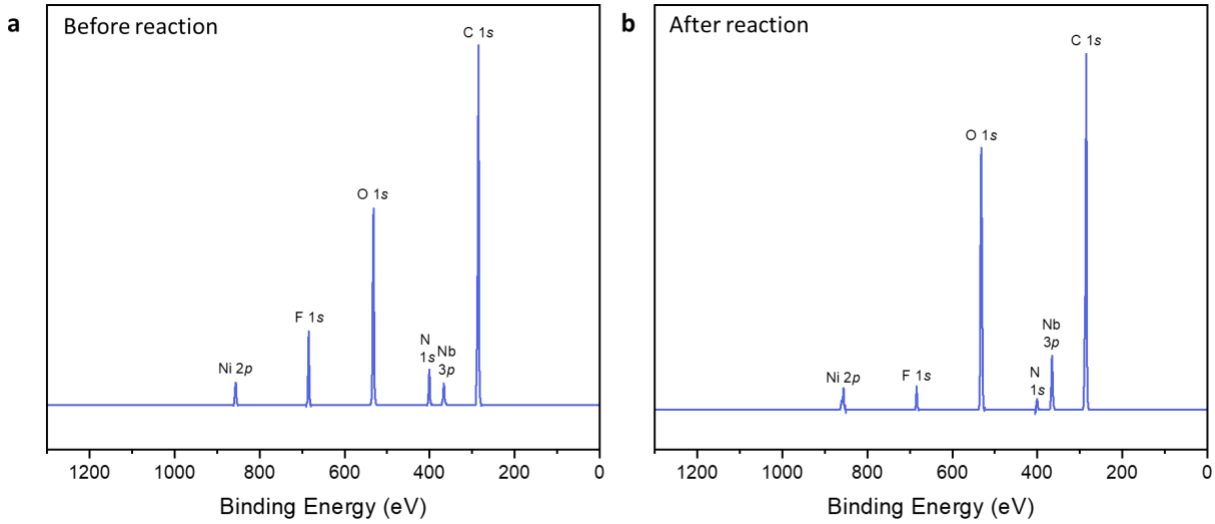

Supplementary Fig. 29. Full XPS scan of Ni-Nb-MOF. a XPS spectrum of Ni-Nb-MOF before reaction. **b** XPS spectrum of Ni-Nb-MOF after reaction.

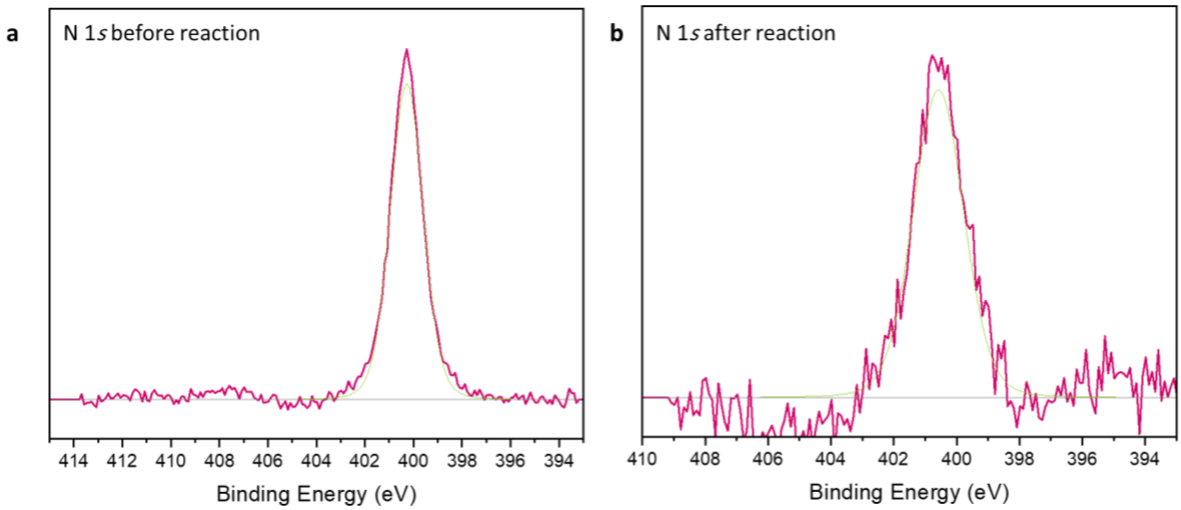

Supplementary Fig. 30. XPS scan of N 1*s* in Ni-Nb-MOF. **a** N 1*s* scan before reaction. **b** N 1*s* scan after reaction. The background is represented as a grey line.

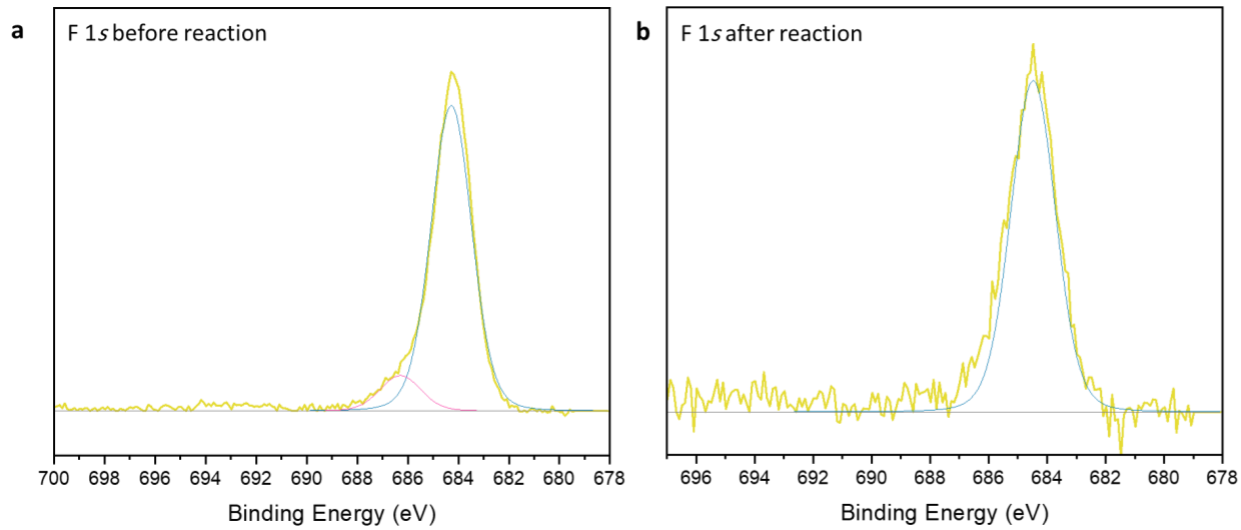

Supplementary Fig. 31. XPS scan of F 1*s* in Ni-Nb-MOF. **a** F 1*s* scan before reaction. **b** F 1*s* scan after reaction. The background is represented as a grey line.

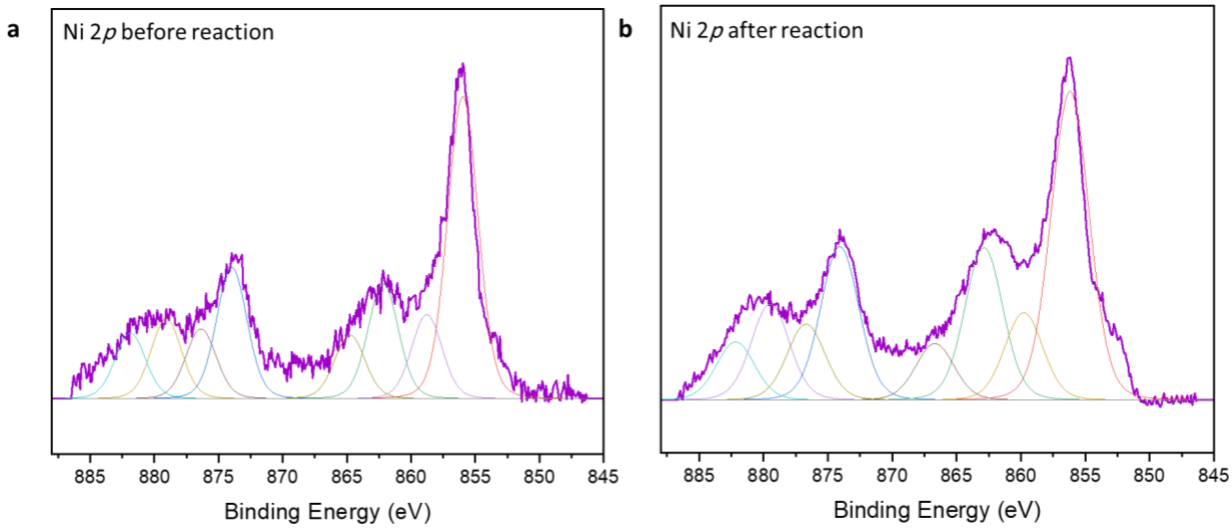

Supplementary Fig. 32. XPS scan of Ni 2*p* in Ni-Nb-MOF. **a** Ni 2*p* scan before reaction. **b** Ni 2*p* scan after reaction. The background is represented as a grey line.

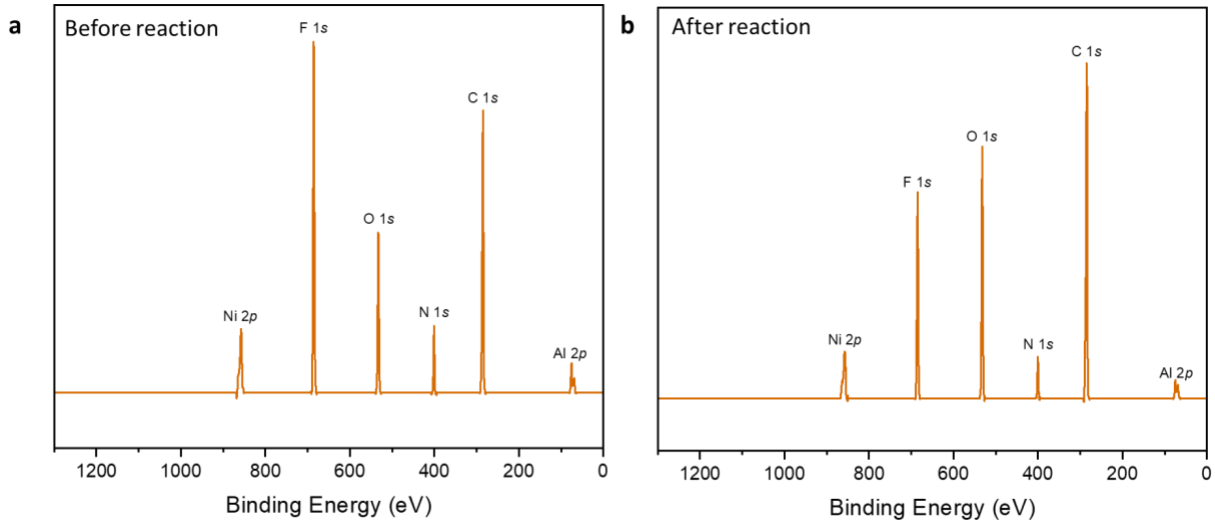

Supplementary Fig. 33. Full XPS scan of Ni-Al-MOF. a XPS spectrum of Ni-Al-MOF before **reaction. b** XPS spectrum of Ni-Al-MOF after reaction.

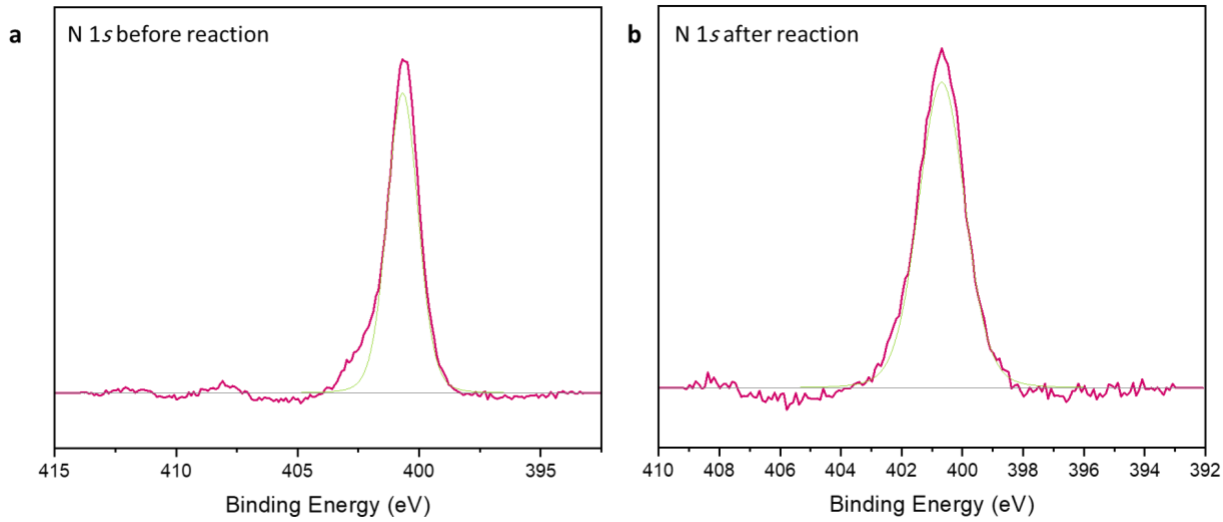

Supplementary Fig. 34. XPS scan of N 1*s* in Ni-Al-MOF. **a** N 1*s* scan before reaction. **b** N 1*s* scan after reaction. The background is represented as a grey line.

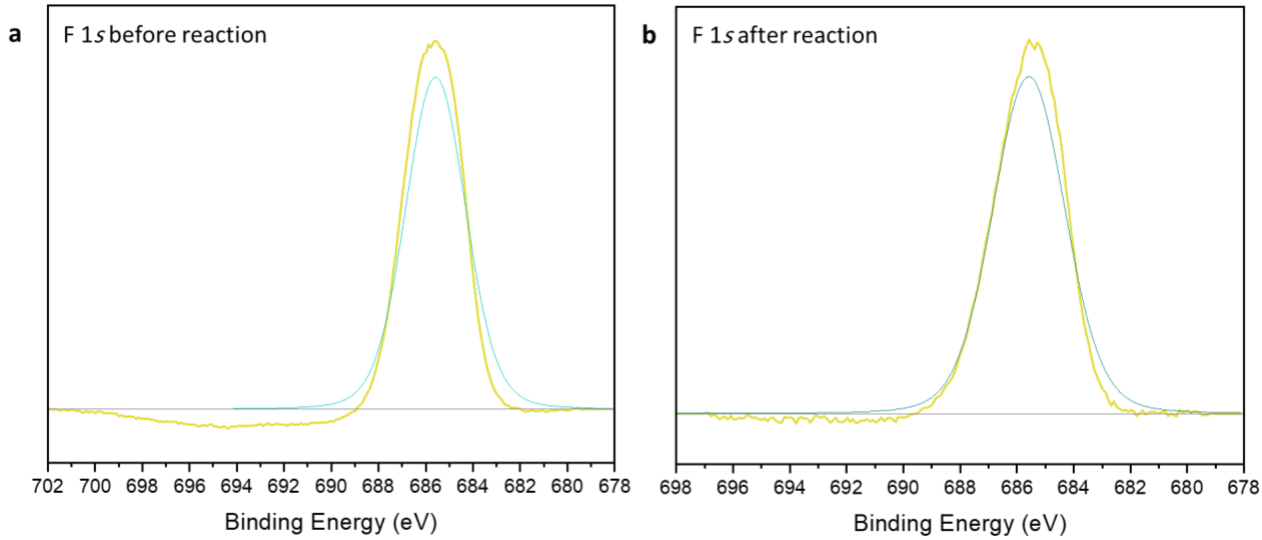

Supplementary Fig. 35. XPS scan of F 1*s* in Ni-Al-MOF. **a** F 1*s* scan before reaction. **b** F 1*s* scan after reaction. The background is represented as a grey line.

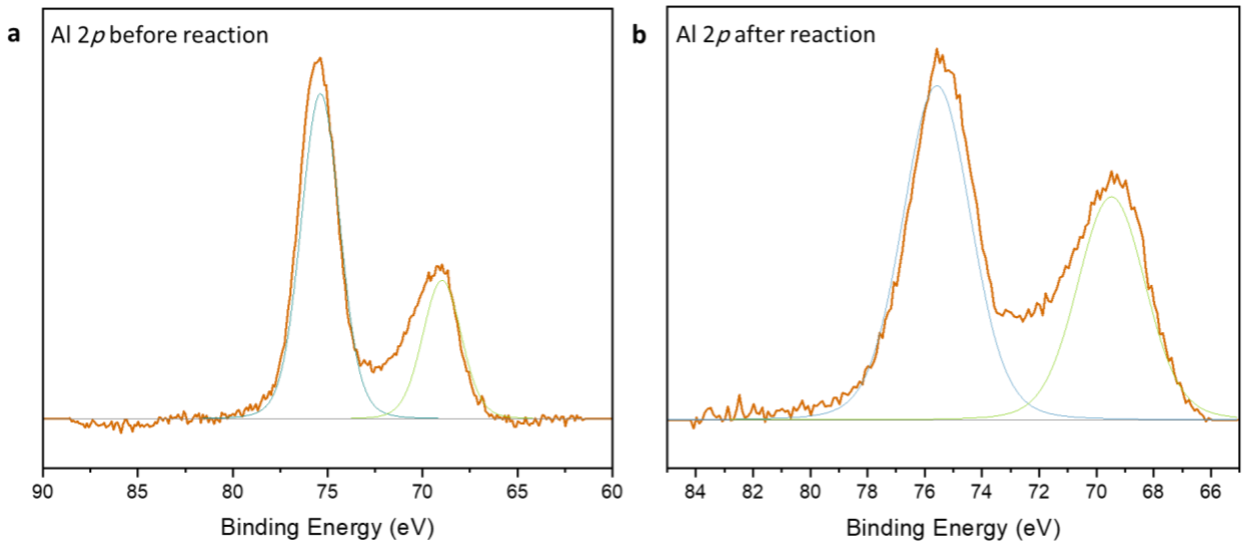

Supplementary Fig. 36. XPS scan of Al 1*s* in Ni-Al-MOF. **a** Al 1*s* scan before reaction. **b** Al 1*s* scan after reaction. The background is represented as a grey line.

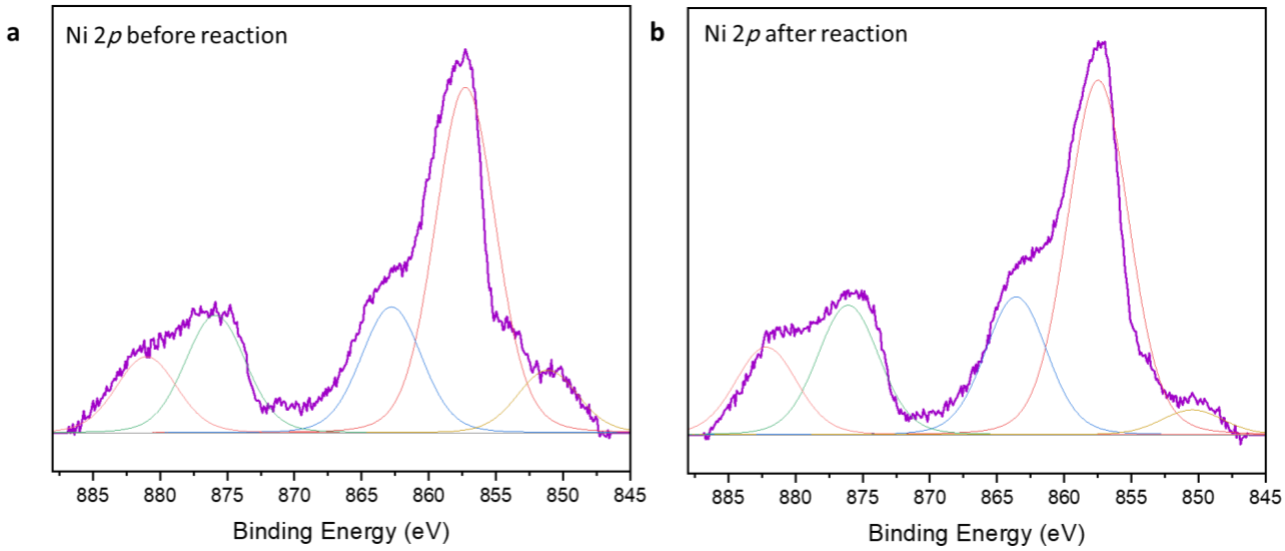

Supplementary Fig. 37. XPS scan of Ni 2*p* in Ni-Al-MOF. **a** Ni 2*p* scan before reaction. **b** Ni 2*p* scan after reaction. The background is represented as a grey line.

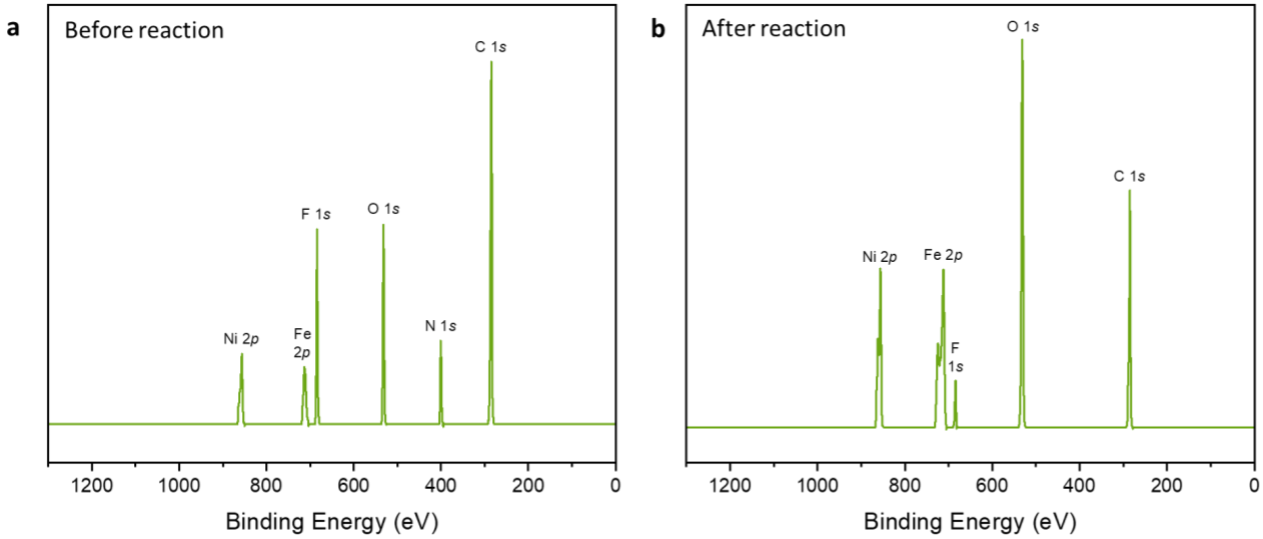

Supplementary Fig. 38. Full XPS scan of Ni-Fe-MOF. a XPS spectrum of Ni-Fe-MOF before reaction. **b** XPS spectrum of Ni-Fe-MOF after reaction.

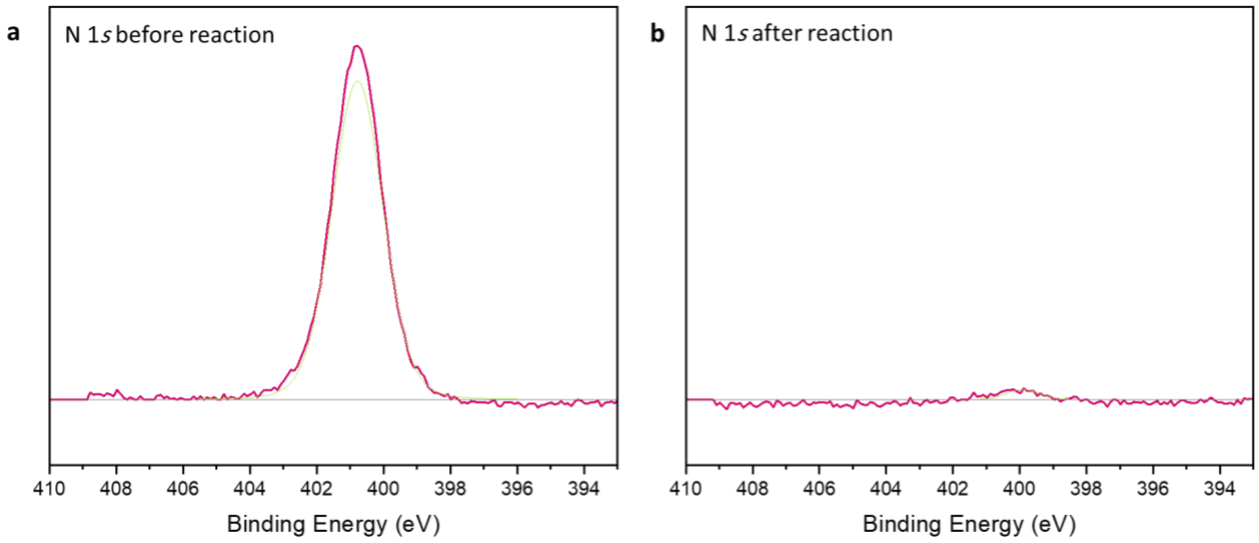

Supplementary Fig. 39. XPS scan of N 1*s* in Ni-Fe-MOF. **a** N 1*s* scan of Ni-Fe-MOF before reaction. **b** N 1*s* scan of Ni-Fe-MOF after reaction. The background is represented as a grey line.

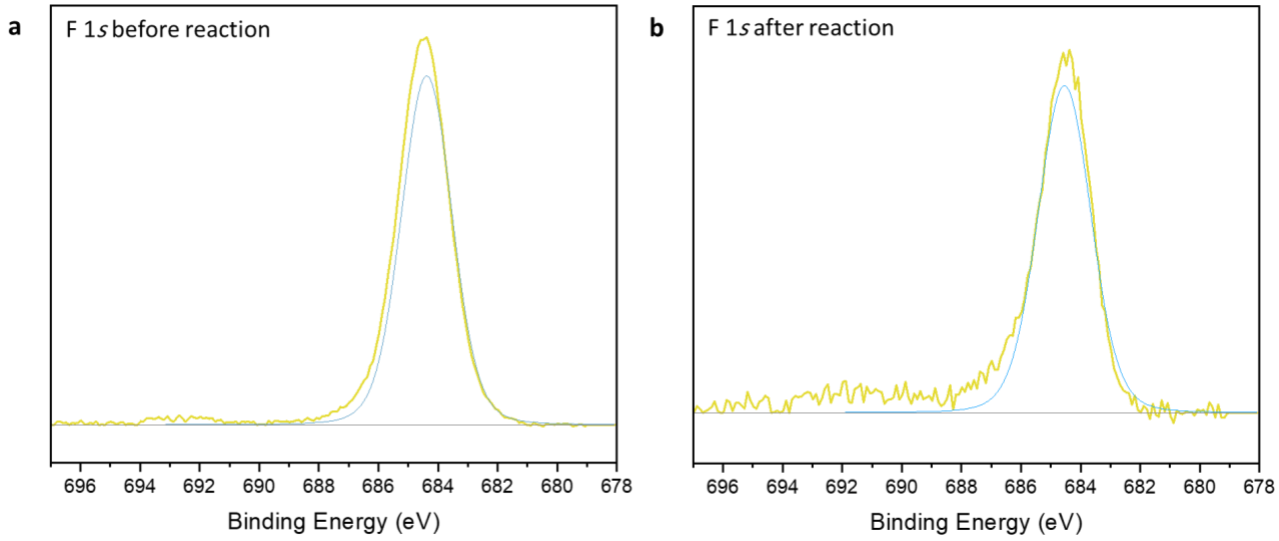

Supplementary Fig. 40. XPS scan of F 1*s* in Ni-Fe-MOF. **a** F 1*s* scan of Ni-Fe-MOF before reaction. **b** F 1*s* scan of Ni-Fe-MOF after reaction. The background is represented as a grey line.

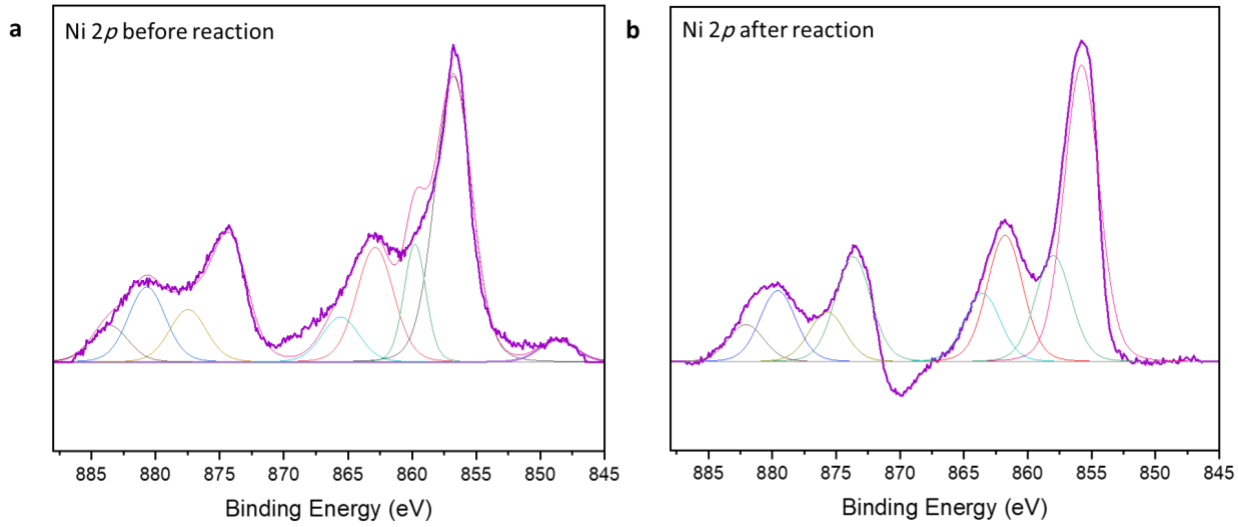

Supplementary Fig. 41. XPS scan of Ni 2*p* in Ni-Fe-MOF. **a** Ni 2*p* scan of Ni-Fe-MOF before reaction. **b** Ni 2*p* scan of Ni-Fe-MOF after reaction. The background is represented as a grey line.